AIAA JOURNAL
Vol. 32, No. 2, February 1994

Numerical Investigation of Mixing Augmentation Behind Oblique Shock Waves

V. I. Vasilev,* S. N. Zakotenko,† S. Ju Krasheninnikov,‡ and V. A. Stepanov§
Central Institute of Aviation Motors, Moscow, Russia

The interaction of a three-dimensional supersonic turbulent jet with an oblique shock wave and a system of shocks in a hypersonic inlet is numerically investigated. The flow is simulated by the parabolized Navier-Stokes equations and a one-equation turbulence model. It is shown that jet convergence behind the single shock leads to an increase of mixing on the order of 2–4 times. The system of shocks in the hypersonic inlet increases the mixing of air and helium injected before the inlet entrance. The mixing completeness at the inlet throat reaches a value of about 0.6–0.7 without significant pressure loss. A simplified technique for estimating the maximum concentration in a jet behind a shock is proposed. The results obtained with the help of this technique agree rather well with the numerical data.

Nomenclature

a	= speed of sound
B, b	= jet width
c	= helium mass concentration
D	= inlet entrance height
d	= jet nozzle height
H	= stagnation enthalpy
L	= characteristic length
M	= Mach number
m	= velocity ratio
n	= static pressure ratio
Pr	= Prandtl number
p	= pressure
Sc	= Schmidt number
u, v, w	= velocity components
$X, Y, Z;$ x, y, z	= Cartesian coordinates
α	= deflection angle
γ	= specific heats ratio
δ	= mixing layer thickness
η	= mixing completeness
μ	= molecular weight
ν	= kinematic viscosity
ρ	= density
σ	= pressure recovery coefficient
ϕ	= angle between shock and x axis

Subscripts

a	= ambient
j	= jet
m	= maximum
T	= total
t	= turbulent

Introduction

TO design an effective scramjet engine one must provide for effective mixing of fuel and air. Generally, to minimize the total pressure loss it is useful to inject gaseous fuel along the air stream direction, but the flow in the scramjet combustion chamber is supersonic and mixing efficiency for coflowing supersonic streams is significantly lower than for subsonic ones.[1] Thus, to increase the mixing efficiency some additional influence must be used. For instance, Drummond et al.[2] suggested the use of longitudinal vortices formed by the lateral edges of a swept wedge fuel injector. Wood et al.[3] used an oscillating shock wave, which influenced the turbulence in the mixing layers; and Naughton et al.[4] used supersonic swirl jets. There also were some other suggestions.

In this work the interaction of a supersonic jet with a stationary oblique shock wave was numerically simulated. Earlier Shau and Dolling[5] experimentally investigated the interaction of an oblique shock with the mixing layer between streams with Mach numbers of 3 and 5 and showed that a stationary shock did not influence the characteristics of the turbulence. Despite the negligible effect of the shock on turbulent transport, it distorts the jet, diminishes its size, and in the three-dimensional case also changes its shape. As our calculations showed, distortion could influence mixing efficiency rather significantly, and the stronger the shock the greater the effect.

Along with the numerical simulations, a simplified technique of estimating the distribution of maximum mass species concentration in a jet interacting with a shock was proposed.

In addition to the interaction of the jet with a single shock, the injection of gas into the hypersonic inlet was also considered. In the latter case the jet interacted with an oblique shock system. Such a pattern could take place if a nontraditional injection mode was used, when fuel is injected before the inlet entrance. Using such a mode one could also decrease the combustion chamber length by shifting the mixing zone upstream. In this work only the mixing process (without burning) was simulated, and thus only nonreactive gases (helium and air) were considered.

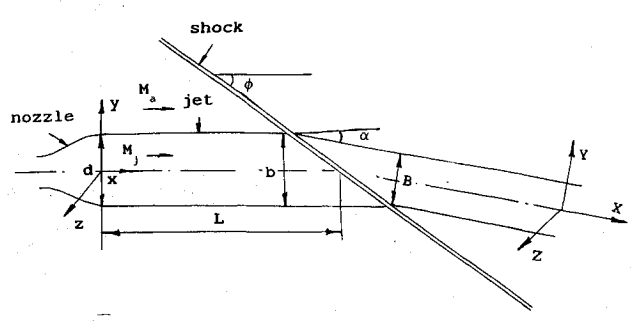

Fig. 1 Schematic diagram of jet interacted with oblique shock.

Received April 29, 1992; revision received April 24, 1993; accepted for publication May 12, 1993.

*Head of Group, Gas Dynamic Department.
†Junior Research Scientist, Gas Dynamic Department.
‡Chief of Department, Gas Dynamic Department.
§Senior Research Scientist, Gas Dynamic Department.

Mathematical Model

In Fig. 1 a schematic of a jet interacting with an oblique shock is presented. Fully expanded supersonic jets of helium, air, or air with a small amount of helium as a passive scalar were injected into a homogeneous unbounded supersonic air stream. Two types of jets were considered: plane jet and square jet. The height of the injected nozzles is d. The origin of the Cartesian coordinates system x, y, z was placed on the jet axis at the nozzle exit. These jets interacted with planar oblique shock waves whose strengths were characterized by the freestream deflection angle α. The angle between the shock in the freestream and the x axis was equal to ϕ. The location of the interaction region was characterized by the parameter L, which equaled the distance between the origin of the coordinate system and the point where the jet axis crossed the undisturbed shock.

A schematic of a helium jet injected into the hypersonic inlet is shown in Fig. 2. Here L is the distance between the jet nozzle exit and the inlet entrance. In Fig. 3 an orthographic projection of the inlet is presented. This hypersonic inlet was designed for a flight Mach number equal to 8 and had a square entrance of height D with a rectangular throat.

In this work only the three-dimensional flows with a supersonic velocity component in the x direction were considered. Such a flow may be described by the parabolized Navier-Stokes equations:

$$\frac{\partial A}{\partial x}+\frac{\partial B}{\partial y}+\frac{\partial C}{\partial z}=\frac{\partial D}{\partial y}+\frac{\partial E}{\partial z}+S \tag{1}$$

$$A=\begin{pmatrix}\rho u\\ \rho u^2+p\\ \rho uv\\ \rho uw\\ \rho uH\\ \rho uc\\ \rho u\nu_t\end{pmatrix},\quad B=\begin{pmatrix}\rho v\\ \rho vu\\ \rho v^2+p\\ \rho vw\\ \rho vH\\ \rho vc\\ \rho v\nu_t\end{pmatrix},\quad C=\begin{pmatrix}\rho w\\ \rho wu\\ \rho wv\\ \rho w^2+p\\ \rho wH\\ \rho wc\\ \rho w\nu_t\end{pmatrix},\quad S=\begin{pmatrix}0\\0\\0\\0\\S_H\\0\\S_\nu\end{pmatrix}$$

$$D=\begin{pmatrix}0\\ \rho(\nu_t+\nu)\dfrac{\partial u}{\partial y}\\ \rho(\nu_t+\nu)\left(\dfrac{4}{3}\dfrac{\partial v}{\partial y}-\dfrac{2}{3}\dfrac{\partial w}{\partial z}\right)\\ \rho(\nu_t+\nu)\left(\dfrac{\partial v}{\partial z}+\dfrac{\partial w}{\partial y}\right)\\ \rho\left(\dfrac{\nu_t}{Pr}+\dfrac{\nu}{Pr}\right)\dfrac{\partial H}{\partial y}\\ \rho\left(\dfrac{\nu_t}{Sc^t}+\dfrac{\nu}{Sc}\right)\dfrac{\partial c}{\partial y}\\ \rho(2\nu_t+\nu)\dfrac{\partial \nu_t}{\partial y}\end{pmatrix},\quad E=\begin{pmatrix}0\\ \rho(\nu_t+\nu)\dfrac{\partial u}{\partial z}\\ \rho(\nu_t+\nu)\left(\dfrac{\partial w}{\partial y}+\dfrac{\partial v}{\partial z}\right)\\ \rho(\nu_t+\nu)\left(\dfrac{4}{3}\dfrac{\partial w}{\partial z}-\dfrac{2}{3}\dfrac{\partial v}{\partial y}\right)\\ \rho\left(\dfrac{\nu_t}{Pr}+\dfrac{\nu}{Pr}\right)\dfrac{\partial H}{\partial z}\\ \rho\left(\dfrac{\nu_t}{Sc^t}+\dfrac{\nu}{Sc}\right)\dfrac{\partial c}{\partial z}\\ \rho(2\nu_t+\nu)\dfrac{\partial \nu_t}{\partial z}\end{pmatrix}$$

In this work the Prandtl number Pr and Schmidt number Sc, as well as the turbulent Prandtl number Pr_t and turbulent Schmidt number Sc_t, were considered invariable and equal to 0.8. The laminar viscosity in the jets was much lower than the turbulent viscosity, so we did not need the precise value of ν, which depends on temperature and gas composition, and thus considered it equal to the laminar viscosity in a homogeneous freestream. The source term in energy and turbulent viscosity equations are given by

$$S_H=\frac{\partial}{\partial y}\left[\left(1-\frac{1}{Pr}\right)\rho(\nu_t+\nu)\frac{\partial q^2}{\partial y}\right]+\frac{\partial}{\partial z}\left[\left(1-\frac{1}{Pr}\right)\rho(\nu_t+\nu)\frac{\partial q^2}{\partial z}\right]$$

$$S_\nu=\rho\nu_t\left[\left(\frac{\partial u}{\partial y}\right)^2+\left(\frac{\partial u}{\partial z}\right)^2\right]^{1/2}\left\{0.2-\frac{5\nu_t}{a^2}\left[\left(\frac{\partial u}{\partial y}\right)^2+\left(\frac{\partial u}{\partial z}\right)^{1/2}\right]^{1/2}\right\}$$

where $q=(u^2+v^2+w^2)/2$. The turbulent viscosity ν_t was determined with the one-equation model.[1]

Helium and air were assumed to be perfect gases with constant specific heats. This assumption is valid for helium over a wide range of temperatures, but for air it may be used only if the temperature is less then 1000 K (Ref. 6). In this work, the latter condition was satisfied in most cases. Using the state equations for a mixture of perfect gases one can derive the equation

$$H=q^2+p/\rho[\gamma_a(1-c)/(\gamma_a-1)+\gamma_j\mu_a c/(\gamma_j-1)/\mu_j]/[(1-c)+\mu_a/\mu_j c]^{1/2} \tag{2}$$

which relates the stagnation enthalpy to the thermodynamic parameters. The γ_a was taken to equal 1.4, γ_j to equal 1.66, and μ_j/μ_a to equal 0.138. It should be noted that in cases where helium was considered to be a passive scalar γ_a and γ_j were both set equal to 1.4, and μ_j/μ_a equal to 1.

PNS equations do not need outflow conditions. At the inflow boundary the distributions of u, v, w, p, H, c, and ν_t must be specified. The form of these distributions for the different variants are discussed subsequently.

When jet/shock interactions were analyzed the computational domain had the form of a rectangular box. The lateral sides of this box were placed at distances such that they did not influence the disturbed flow area. At these boundaries the nonreflecting conditions were specified (i.e., the parameters here had the same values as the incoming characteristics).

When the problem of injection into an inlet was analyzed, the freejet was simulated first; then the flowfield in section x, corresponding to the prescribed distance L, was chosen as the inflow conditions at the entrance of the inlet. On the inlet

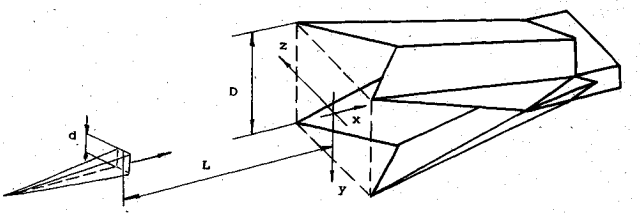

Fig. 2 Schematic diagram of helium jet blowing into the hypersonic inlet.

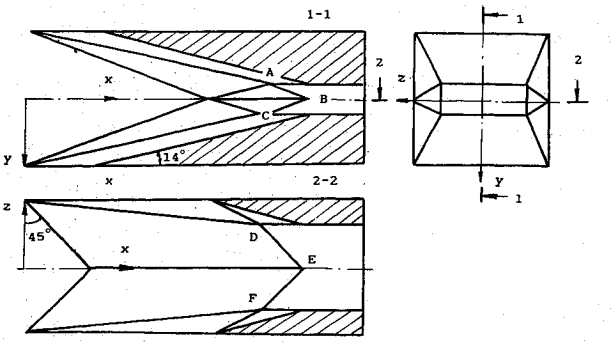

Fig. 3 Draft of hypersonic inlet.

walls the slip conditions were specified (i.e., the wall boundary layers were not taken into account). This approach was partially justified, since the jet axis was coincident with inlet axis and the lateral extent of the jet did not reach the walls.

Equations (1) and (2) were integrated numerically by the explicit finite-difference method. The convective terms [left-hand side of Eqs. (1)] were approximated by the modified Godunov scheme.[7] This modification, proposed by Kolgan,[8] made the scheme monotonic and second order in the cross directions (i.e., this is a kind of total variational diminishing scheme). The diffusion terms [right-hand side of Eqs. (1)] were approximated by a central difference scheme.

The resulting scheme was conservative, second-order accurate in the transverse direction, and first-order accurate in the longitudinal direction. Most calculations for the jet/shock interaction were performed using 80×80 cells in each cross section; but for the inlet, the typical grid contained 40×40 cells.

Jet/Shock Interaction

A. Verification of Mathematical Model

To check the algorithm and computational codes some test calculations were made. These tests included: inviscid two-dimensional flow around the wedge, for which analytical solutions exist; inviscid three-dimensional flow in the corner, formed by the junction of two wedges, for which the numerical results had been obtained by Charwat and Reclekopp[9]; and a circular turbulent supersonic jet issuing into a supersonic stream, for which experimental data exist.[10] The agreement between our calculations and the analytical or known numerical results was very good. The agreement with experimental data was also reasonable.

The most suitable data for verifying the jet/shock interaction model were obtained by Shaw and Dolling.[5] They investigated the plane air jet with Mach number $M_j = 3$ issuing into the air stream with $M_a = 4.9$. The ratio of the static pressure in the jet to that in the air stream ($n = p_j/p_a$) was about 1, whereas the ratio of velocities ($m = u_a/u_a$) was equal to 1.23.

The velocity profiles at the nozzle exit plane were nonuniform due to the boundary layers, but the temperature profile in each stream was practically uniform. The jet interacted with a planar shock wave, with $\alpha = 6$ deg, at a distance $L/d = 2.62$.

In the numerical simulation of this flow the pressure distribution at the nozzle exit plane was uniform; the temperature profiles in the jet and the stream were also uniform (however temperatures in each stream were different); the cross velocities were equal to zero ($v = w = 0$); and the u profile was

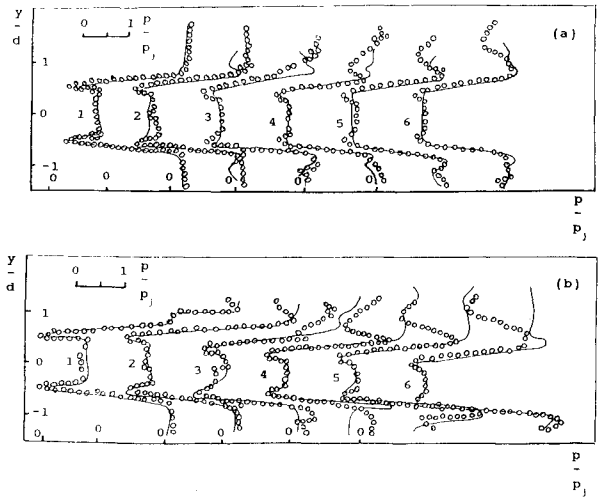

Fig. 4 Pitot pressure profiles (analysis, ——, and experiment,[5] o); 1) $x/d = 0$, 2) $x/d = 1.33$, 3) $x/d = 2.62$, 4) $x/d = 4.0$, 5) $x/d = 5.36$, 6) $x/d = 6.68$: a) undisturbed air jet and b) air jet interacted with oblique shock.

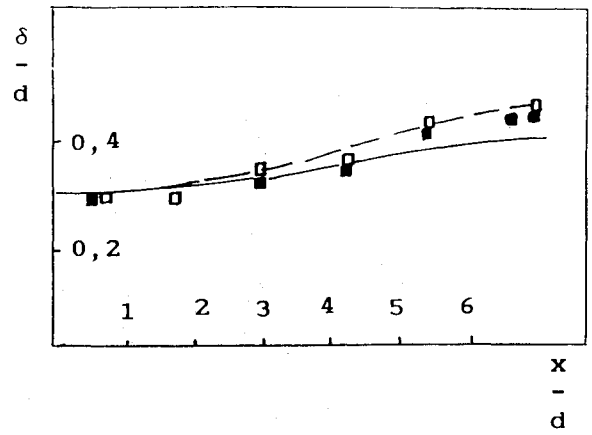

Fig. 5 Thickness of upper mixing layer of the freejet (analysis, – – –, and experiment,[5] □) and of the interacted jet (analysis, ——, and experiment, ■).

taken from the experiment. Using this data one could also calculate the distribution of stagnation enthalpy H. The profiles of ν_t in Ref. 5 were not measured. However, the u-velocity distribution in the boundary layers was the same as that in a boundary layer on a flat plate, and so for turbulent viscosity we could use the data obtained by other authors for the flat plate boundary layer.[11] The maximum value of ν_t at the nozzle exit plane was $\nu_t/u_a d = 1.5E - 4$.

The comparison between the calculated and the measured results are presented in Fig. 4, where the pitot pressure profiles at different longitudinal locations are shown. Figure 4a shows profiles in the freejet whereas Fig. 4b shows profiles at the jet/shock interaction. The agreement between experiment and computation is rather good. Some discrepancies downstream of the shock are due to disturbances from the nozzle lip, which in reality had finite thickness.

In Fig. 5 the thicknesses of the upper mixing layer are presented. The thickness δ is the distance between points where the pitot pressures differ by 5% from the pressure in the core streams. The agreement between experiment and computation is rather good. The shock did not influence the mixing layer thickness (i.e., it did not change the turbulent transport). This result was also confirmed by the calculated ν_t distribution. However, downstream of the shock the jet potential core lateral extent is diminished (i.e., the jet is converged), as can be seen from Fig. 4b. The mixing layer thicknesses do not change, but the distance between layers is diminished, and thus the mixing effectiveness is increased. A clearer picture of the effect of mixing augmentation may be seen in the three-dimensional helium jet.

B. Three-Dimensional Helium Jet

The flow around the square nozzle was not simulated. The distributions of u, p, H, and c at the nozzle exit and in the freestream at the same x station were assumed to be uniform, and cross velocities were taken to be zero. The basic parameters were varied in the range: $M_a \leq 8$, $2 \leq M_j \leq 12$, and $1 \leq n \leq 1.4$. The velocity ratio was 2 and the shocks were characterized by $\phi = 14$ and 7 deg.

The distance L was approximately equal to the length of the potential core ($L = 40d$). The length of the potential core was defined as the distance between the nozzle exit and the x station where the maximum concentration c_m differed from 1 by 1%. The width b was defined as the distance between two points in the symmetry plane where $c = 0.05c_m$.

When the velocity ratio $m = 2$ and the boundary layers at the nozzle exit are thin, the level of turbulent viscosity at the end of the potential core is determined mainly by turbulence generation in the mixing layers and weakly depends on the initial viscosity level at the nozzle exit. In our case the maxi-

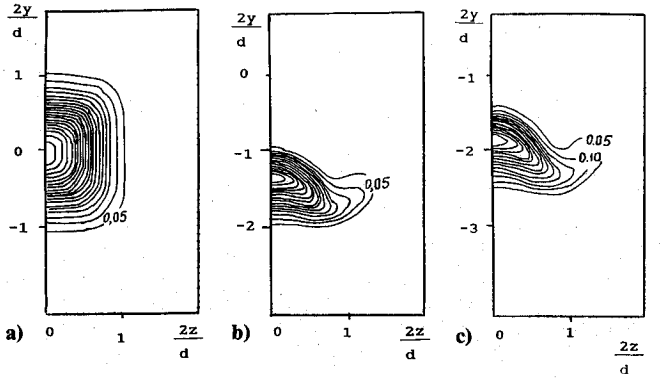

Fig. 6 Contours of helium concentration: a) $x/d = 40.44$, b) $x/d = 51.1$, and c) $x/d = 53.3$.

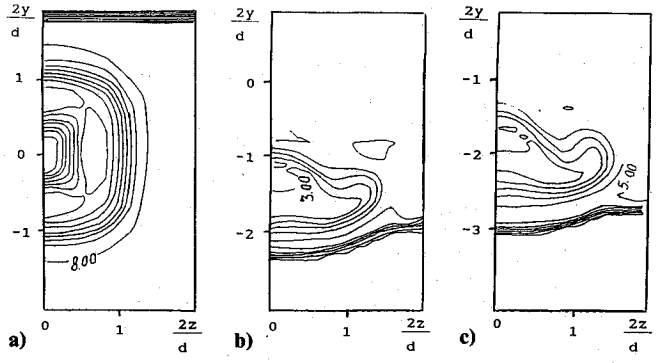

Fig. 7 Contours of longitudinal Mach number: a) $x/d = 40.44$, b) $x/d = 51.1$, and c) $x/d = 53.3$.

mum level of $\nu_t/u_a d$ at the nozzle exit was equal to $1.7E-4$, and at the end of the potential core was equal to $2.3E-3$. The one-equation model[1] describes the process of turbulence generation rather well, so our choice of L and $m = 2$ removed the arbitrariness of ν_t in interaction region, even if we did not simulate the flow around the jet source.

The calculations have shown that the main characteristic features of square jet/shock interactions are as follows.

1) The turbulent viscosity is essentially unchanged behind the shock as in the planar air jet.

2) The jet is converged in the y direction, and the degree of convergence mainly depends on angles ϕ and α. If one introduces the degree of convergence as b/B, where b is the jet width before the shock and B is the jet width behind shock, then $B/b \sim \sin(\phi - \alpha)/\sin\phi$ (this relationship is illustrated in Fig. 1).

3) In addition to jet convergence, which also takes place in a planar jet, the square helium jet is distorted due to secondary flows.

The distortion is shown in Figs. 6 and 7. In Fig. 6 the contours of concentration lines of helium for the $M_a = 8$ case are shown. A map of the contours in the station before the shock is presented in Fig. 6a and the stations behind the shock in Figs. 6b and 6c. Because of symmetry only half-planes are shown. The step between contours $\Delta c = 0.05$. Figures 7a–7c show the longitudinal Mach number contours ($M_x = u/a$) for the same case. It should be noted that for all helium jets considered, the contour patterns had analogous horseshoe shapes.

The horseshoe shape of the jet cross section is a result of secondary flows that are generated by longitudinal vortices formed behind the shock. The mechanism of this vortex generation is twofold. One mechanism is the baroclinic effect, which is due to the presence of a pressure gradient in the flow direction and a density gradient in the cross direction in the jet/shock interaction region. The second mechanism is streamline turning into the shock. Due to this effect, the vorticity, which has only cross components in freejet, acquires the longitudinal component behind the shock. This secondary vorticity is strong enough to distort the jet cross section, but its influence on mixing effectiveness is small.

Mixing effectiveness may be characterized by the maximum concentration value c_m. Figure 8 presents the distribution of c_m in a freejet (curve 1) and in a jet interacted with shock (curve 2) for the case discussed previously. To clarify the role of secondary flows, the diffusion of the passive scalar behind the source of a square cross section in an undisturbed flow with the planar shock ($M_a = M_j = 8$, $n = m = 1$) was also simulated. In this case there were no secondary flows and the distribution of ν_t was taken from the helium jet calculation. The relation of c_m via $x_s = (x - L)/d$ for this case is also plotted in Fig. 8 (curve 3). Comparison of the three curves shows that mixing behind the shock increases rather significantly and that mixing augmentation is due to jet convergence rather than to secondary flows. Comparison of curves 2 and 3 also shows that for mixing effectiveness estimation a simplified method can be used.

C. Simplified Estimation of Maximum Concentration

Assuming that the diffusion coefficient ν_c is constant, one can obtain the asymptotic ($x/d \gg 1$) relations for passive scalar concentration behind a square source in a homogeneous stream:

$$c_m(x) = d^2 u_a/4\pi\nu_c x \tag{3}$$

$$c = c_m(x)\exp(-y^2/b^2 - z^2/b^2), \qquad b^2 = 4\nu_c x/u_a \tag{4}$$

Let us also assume that just downstream of the shock, the distribution of c in coordinates X, Y, Z, rotated by the angle α, has the form of Eq. (4), but with different widths in the Y and Z directions

$$c = c_{ms}\exp(-Y^2/B^2 - Z^2/b^2) \tag{5}$$

where the ratio B/b is connected with shock angles α and ϕ by

$$B/b = \sin(\phi - \alpha)/\sin(\phi) \tag{6}$$

As mentioned earlier, this relationship also approximately describes the degree of convergence for a helium jet.

For a passive scalar jet in a homogeneous stream with c initial distribution given by Eq. (5), the asymptotic distribution of maximum concentration is given by

$$c_m = c_{mS}\frac{bBU}{4\nu_c X} \tag{7}$$

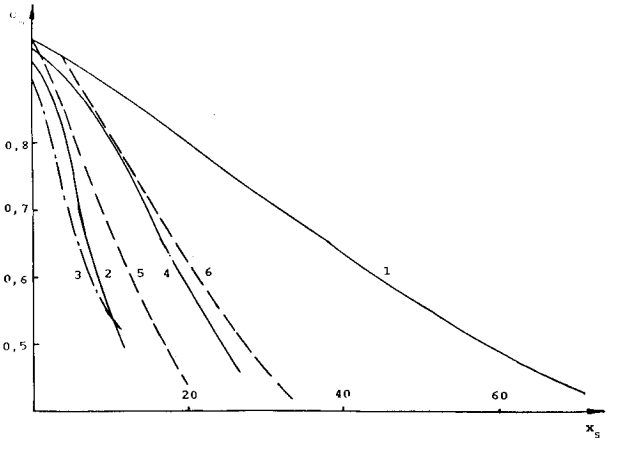

Fig. 8 Maxium concentration: 1) a free helium jet; 2) the numerical calculation (helium jet), $\phi = 14$ deg; 3) the numerical calculation (passive scalar), $\phi = 14$ deg; 4) the numerical calculation (helium jet), $\phi = 7$ deg; 5) the simplified estimate, $\phi = 14$ deg; and 6) the simplified estimate, $\phi = 7$ deg.

The velocity behind the shock U is connected with parameters before the shock by Rankine-Hugoniot relations, and thus u/U is a function of ϕ and M_a. It must be noted that when using the Rankine-Hugoniot relations the ratio B/b, given by Eq. (6), also may be presented as a function of ϕ and M_a.

When the angle α is small and x is large then X in Eq. (7) may be replaced by x. In that case one can get Eq. (7) from Eq. (3) by substituting $x^0 = x(b/B)(u_a/U)$ in Eq. (3) for x. Based on this last remark one can propose a simplified technique for maximum concentration estimation: if $c_{m0}(x)$ is the maximum concentration in a freejet, then behind the shock the maximum concentration is given by

$$c_m(x) = c_{m0}(\xi) \tag{8}$$

where $\xi = x(u_a/U)\,[\sin\phi/\sin(\alpha - \phi)]$ and may be calculated from the Rankine-Hugoniot relations. Although the relation (8) was obtained for a passive scalar, it could also be used for the estimation of helium concentration. In the latter case, one must calculate the c_{m0} distribution in a free helium jet; and then using Eq. (8), the c_m distribution behind oblique shocks with different strengths, determined by M_a and ϕ, may be estimated. It should be noted that the simplified technique (8) also may be used for round and rectangular jets with moderate aspect ratios.

To verify the simplified method, the results obtained with the help of Eq. (8) are compared with the numerical simulation data in Fig. 8. The jet parameters are the same, and two shocks of different strengths are considered. These comparisons show that the approximated results agree with numerical data rather well. In addition, the figure also shows that the oblique shock augments mixing rather significantly with peak c_m decreasing at a rate 2–4 times faster than the freejet.

Jet Injected into Inlet

The hypersonic inlet shown in Fig. 3 was designed for a flight Mach number of 8. To find the main characteristics of this inlet at design conditions, the flow without injection was simulated first.

In Fig. 9 maps of isobars at different sections are presented (due to the symmetry only one-quarter of a section is shown). The pressure here is normalized by $\rho_a u_a^2$. Analysis of these and analogous pictures in other sections show that there are no slots between the first shock and the side wedges, and consequently there are no overflows around these wedges and the discharge coefficient is equal to 1. The shock reflects from the symmetry plane, then approximately traces the sharp bend on the side wall (lines AB and BC in Fig. 3), and finally comes to

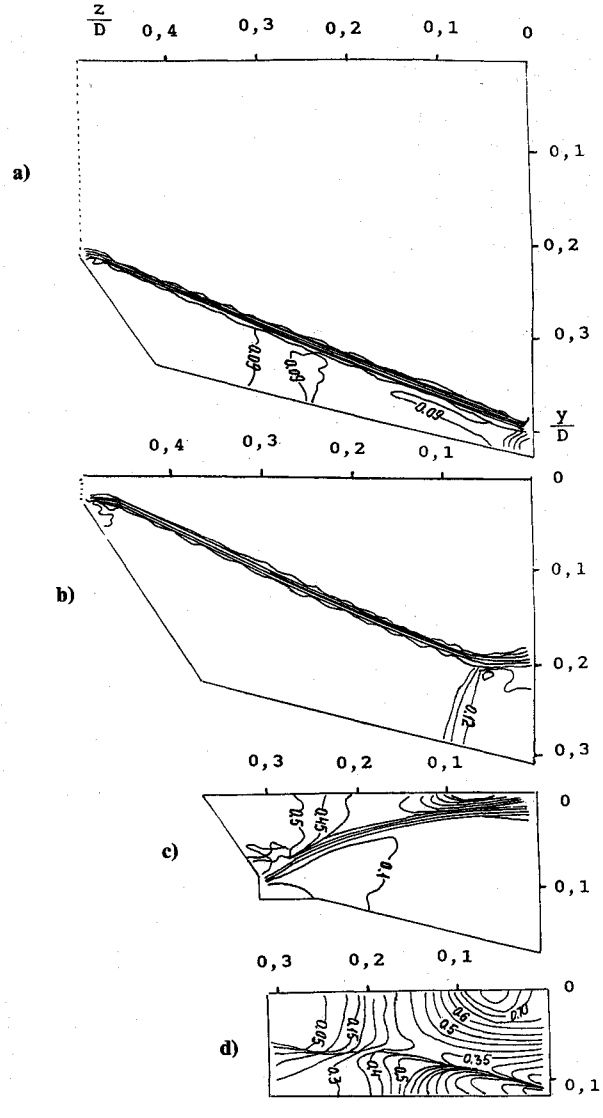

Fig. 9 Contours of pressure: a) $x/D = 0.75$, b) $x/D = 1.25$, c) $x/D = 1.83$, and d) $x/D = 2.25$.

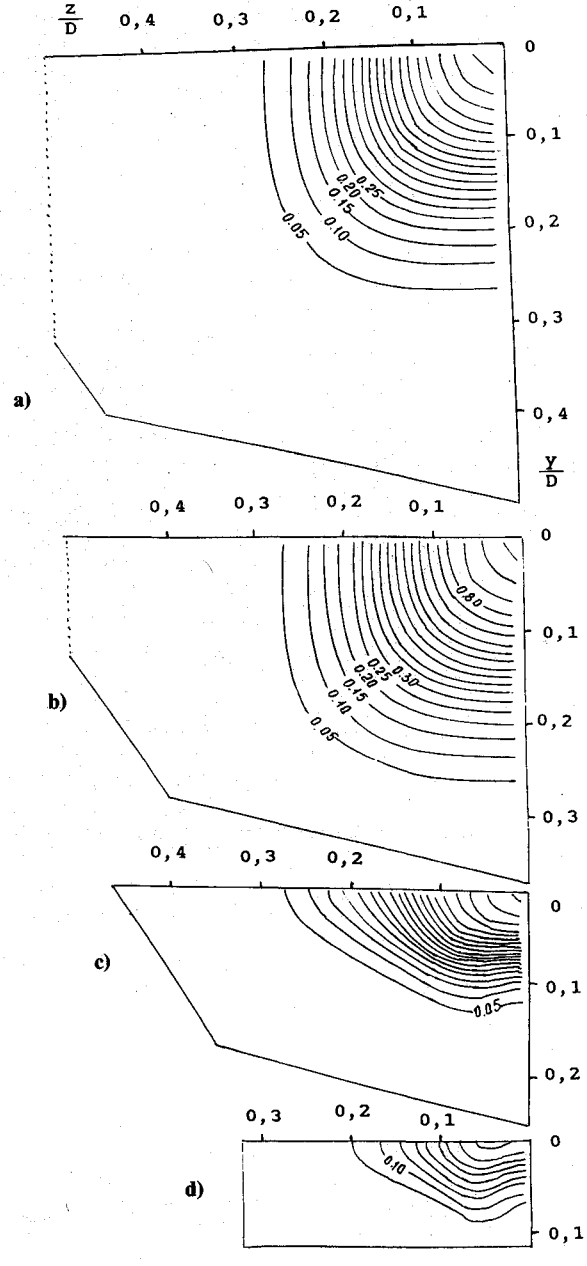

Fig. 10 Contours of helium concentration: a) $x/D = 0.5$, b) $x/D = 1.0$, c) $x/D = 1.5$, and d) $x/D = 2.5$.

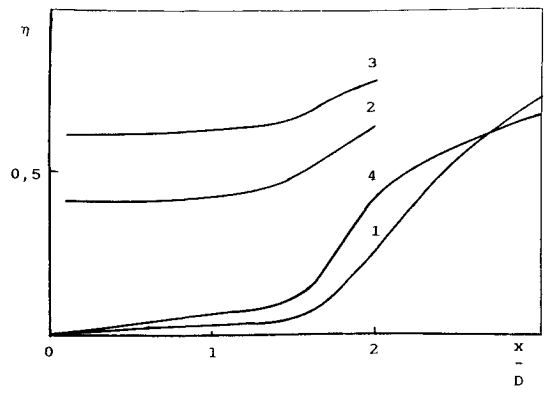

Fig. 11 Mixing completeness: 1) $L/D = 9$, 2) $L/D = 20$, 3) $L/D = 27$, and 4) the passive scalar ($L/D = 9$).

the sharp bend on the bottom wall (lines DE and EF in Fig. 3). The reflected shocks in the throat are rather weak. The full length of the inlet is equal to $\Delta x/D = 2.5$, thus the last picture in Fig. 9 corresponds to the final inlet section. This inlet has a rather high-pressure recovery coefficient. If σ is defined as $\sigma = \overline{p}_T / p_{Ta}$, where $\overline{p}_T$ is the total pressure averaged at given station by the rule

$$\overline{p}_T = \int p_T \rho u \, dy \, dz / \int \rho u \, dy \, dz$$

then at the final inlet station σ is equal to 0.22.

The initial parameters of the helium jet injected into the inlet were the same as those of the previously discussed case (i.e., $M_a = 8$, $M_j = 6.9$, $n = 1.36$, $m = 2.0$). This case used a square jet, but the flow around the source of the jet was not simulated. The jet axis coincided with the inlet axis. A set of distances between the jet nozzle exit and the inlet entrance in the range $L/D = 9$–27 were considered. As mentioned earlier, at these distances from the jet nozzle, the viscosity is mainly determined by turbulence generation and is practically independent of the initial level of ν_t.

It also should be noted that if one maintains the jet parameters M_j, n, and m, but replaces helium with hydrogen, then the mass flow rates of hydrogen and air passing through the inlet are in a stoichiometric ratio. On the other hand, the similarity of the parameters M_j, n, and m ensure the similarity of turbulent mixing, thus the results presented subsequently may be used to estimate the mixing of fuel and air in stoichiometric conditions.

The structure of the helium jet passing through the inlet is illustrated in Fig. 10, where the contours of concentration lines are shown. These data were obtained for $L/D = 9$. Near the inlet entrance, the jet and leading shock are separated. Then the jet/shock interaction occurs. Passing through the system of shocks, the helium spreads in the y direction over the entire span of the throat. However, in this case a rather strong crossflow in the z direction removes the horseshoe shape.

The discharge coefficient here was equal to 1, and all of the helium passed through the inlet. The mixing effectiveness may be characterized by the mixing completeness η, determined by the relationship

$$\eta = (1 - c_m)/(1 - \overline{c})$$

where c_m is the maximum concentration at the given x station, and $\overline{c}$ the concentration at full mixing. The distributions of η along the inlet passage for three different values of L are presented in Fig. 11. It is seen that mixing completeness in the throat can reach rather high values of about $\eta = 0.6$. Curves 2 and 3 are broken off at $x/D = 2$ because downstream of this location small subsonic zones arose and calculations could not be continued.

When $L/D = 9$ the additional pressure loss due to mixing is small, and σ in the throat is diminished from 0.22 to 0.18. In the other two cases ($L/D = 20$ and 27) the additional losses were more significant ($\sigma = 0.11$ and 0.08 at $x/D = 2$ and less in the throat), but the increase of mixing is small, and so one can conclude that there are optimum values of distance between the inlet and jet nozzle. To find this optimum, one must include the losses due to the jet injector in the analyses.

Conclusions

The interaction of a three-dimensional supersonic turbulent jet with an oblique shock wave and a system of shocks in an inlet was numerically investigated. The flow was modeled by the parabolized Navier-Stokes equations and a one-equation turbulence model.

The calculations showed that a square jet of helium or air with a passive scalar fully expanded jet converged behind the oblique shock. The turbulent viscosity behind the shock was not changed, but the convergence due to the shock led to an increase in mixing. The peak concentration in the jet/shock interaction decreased at a rate 2–4 times faster than that of the freejet. In the helium jet, vortex secondary flows were also generated which distorted the jet into a horseshoe shape.

A simplified technique for the estimation of maximum concentration in a jet behind a shock was proposed. The results obtained with the help of this technique agree rather well with the numerical data.

The system of shocks in a hypersonic inlet designed for a flight Mach number of 8 significantly increases the mixing of air and helium injected upstream of the inlet entrance. The mixing completeness in the inlet throat reaches a value of 0.6–0.7 with a rather small additional pressure loss. The pressure recovery coefficient is reduced from 0.22 in the flow without injection to 0.18 in the flow with it.

References

[1]Kozlov, V. E., Secundov, A. N., and Smirnova, I. P., "The Model of Turbulence for Simulation of Compressible Gas Jet Flow," *Izvestiya Akademii Nauk SSSR, Mech. Zhid. i Gaza,* No. 6, 1986, pp. 38–44.

[2]Drummond, J. P., Carpenter, M. H., Riggins, D.W., and Adams, M. S., "Mixing Enhancement in a Supersonic Combustor," AIAA Paper 89-2794, July 1989.

[3]Wood, C. W., Thomas, R. H., Schetz, I. A., "Effects of Oscillating Shock Impingement on the Mixing of a Gaseous Jet in a Mach 3 Airstream," AIAA Paper 90-1982, April 1990.

[4]Naughton, J. W., Cattafesta, L. N., Settles, G. S., "An Experimental Study of the Effect of Streamwise Vorticity on Supersonic Mixing Enhancement," AIAA Paper 89-2456, July 1989.

[5]Shau, Y. R., Dolling, D. S., "Experimental Study of Spreading Rate Enhancement of High Mach Number Turbulent Shear Layers," AIAA Paper 89-2458, July 1989.

[6]Predvoditelev, A. S., Stupachenko, E. V., Pleshanov, A. S., Samuilov, E. V., and Rozdestvensky, I. B., "The Tables of Thermodynamics Functions for Air," Vychislit. Center Akad. Nauk SSSR, Moscow, 1962.

[7]Godunov, S. K., et al., *Numerical Simulation of Multi-Dimensional Gasdynamics Problems,* Nauka, Moscow, 1976.

[8]Kolgan, V. P., "Finite-Difference Scheme for Calculation of Unstationary Two-Dimensional Discontinued Gasdynamics Solutions," *Uchenye Zapiski TzCAGI,* Vol. 6, No. 1, pp. 9–14.

[9]Charwat, A. F., Reclekopp, J. Q., "Supersonic Interference Flow Along the Corner of Intersecting Wedges," *AIAA Journal,* Vol. 5, No. 3, 1967.

[10]Abramovich, G. N., *Turbulent Jets,* Nauka, Moscow, 1984.

[11]Hinze J. O., *Turbulence,* McGraw-Hill, New York, 1975.